Dopant-Free, Novel Hole Transporting Materials Based on Quinacridone Dye for High-Performance and Humidity Stable Mesoporous Perovskite Solar Cells

Hong Duc Pham,[a]† Sagar M. Jain,[b*]† Meng Li,[b,c] Sergei Manzhos,[e] Krishna Feron,[f,g] Sudhagar Pitchaimuthu,[b] Zhiyong Liu,[h] Nunzio Motta,[a] Hongxia Wang,[a] James R. Durrant,[b,d] Prashant Sonar[a*]

a. Institute of Future Environment and School of Chemistry, Physics and Mechanical Engineering, Queensland University of Technology (QUT), 2 George Street, Brisbane, QLD-4001, Australia.

b. SPECIFIC, College of Engineering, Swansea University Bay Campus, Fabian Way, SA1 8EN Swansea, United Kingdom.

c. Jiangsu Key Laboratory for Carbon-Based Functional Materials and Devices, Institute of Functional Nano and Soft Materials (FUNSOM), Soochow University, Suzhou 215123, China.

d. Department of Chemistry and Centre for Plastic Electronics, Imperial College London, Exhibition Road, London SW7 2AZ, United Kingdom.

e. Department of Mechanical Engineering, Faculty of Engineering, National University of Singapore.

f. CSIRO Energy Centre, NSW-2304, Australia.

g. Centre for Organic Electronics, University of Newcastle, Callaghan, NSW 2308, Australia.

h. Department of Physics and Materials Science, Henan Normal University, Henan Key Laboratory of Photovoltaic Materials, Xinxiang 453007, China

† These authors, H. D. P and S. M. J contributed equally to the work.

Electronic Supplementary Information (ESI) available: [details of any supplementary information available should be included here]. See DOI: 10.1039/x0xx00000x

Email i.d. of corresponding authors sonar.prashant@qut.edu.au and sagarmjain@gmail.com or s.m.jain@swansea.ac.uk

Abstract

This work reports three newly developed dopant free hole transporting materials (HTMs) for perovskite solar cells. The design is based on quinacridone (QA) dye as a core with three different extended end-capping moieties including acenaphthylene (ACE), triphenylamine (TPA) and diphenylamine (DPA) attached to the QA. These HTMs were synthesized and fabricated successfully in mesoscopic TiO_2/$CH_3NH_3PbI_3$/HTM perovskite devices. Under 100 mW cm^{-2} AM 1.5G, the devices achieved a maximum efficiency of 18.2% for **ACE-QA-ACE**, 16.6% for **TPA-QA-TPA** and 15.5% for **DPA-QA-DPA** without any additives, while the reference devices with doped Spiro-OMeTAD as HTM showed a PCE of 15.2%. Notably, the unencapsulated devices based on these novel dopant-free HTMs show impressive stability in comparison with the doped Spiro-OMeTAD devices under 75% relative humidity for 30 days. These linear symmetrical HTMs pave the way to a new class of organic hole transporting materials for cost-efficient and large area applications of printed perovskite solar cells.

Keywords: quinacridone, acenaphthylene, triphenylamine, dopant-free, perovskite solar cells

Introduction

The research efforts related to π-conjugated vat dyes and pigments are burgeoning because of their outstanding properties such as the fused planar aromatic hydrocarbon nature, high backbone rigidity, backbone planarity of the core structures, strong absorption in the visible range, high environmental, thermal and chemical stability and the possibility to tune optoelectronic properties via functionalization with functional groups like ketones, halogens and amines.[1, 2] Additionally, some of them are very cost-efficient such as carbazole, anthanthrone, quinacridone and so forth. Currently, this type of materials has been employed intensively in organic solar cells (OSC), organic light-emitting diodes (OLEDs), sensors and organic field-effect transistors (OFETs).[1-5]

Particularly, the use of inexpensive organic dyes as hole transporting materials (HTMs) for perovskite solar cells (PSCs) has attracted attention because it opens a new way for the development of cost-effective and printable solar cells. Recently, HTM designs based on anthanthrone (ANT),[3, 4] carbazole (CAZ),[6-8] diketopyrrolopyrrole (DPP),[9, 10] and isoindigo (IS)[11] dyes exhibited promising power conversion efficiencies (PCE) in perovskite devices. Several dye based HTMs are reported in the literature but most of them used dopant as an additive to enhance the power conversion efficiency of PSC.[7, 8] Though the PCE is enhanced, the presence of salt dopants leads to the decrease in the stability of the devices and the increase in the cost of production. Therefore, the development of novel dopant-free organic dyes-based HTMs is important. As per our knowledge, there are not much reports about using dopant free dyes as a hole tranpsorting materials for perovskite solar cells in the literature.

Owing to the high chemical and thermal stability, low cost, planar fused molecular structure, intermolecular hydrogen bond and high charge carrier mobility, in our current work we explored the used of quinacridone (QA) dye as core for the development of new class of HTMs for PSC technology. It has been well documented that QA dye and its derivatives have been widely employed as an active semiconductor in various optoelectronic devices, including organic solar cells, light-emitting diodes, sensors and field-effect transistors.[2, 12-17] Nevertheless, its use in PSCs has not yet been reported. Interestingly, QA is a well-known acceptor material due to presence of two electron withdrawing ketonic groups in the conjugated backbone. Electron withdrawing QA

skeleton leads to a low-lying highest occupied molecular orbital (HOMO) level, which minimizes the energy offset between the valence band maximum of perovskite and the HOMO of hole transporting layers. This boosts the open circuit voltage (V_{oc}) and the efficiency of PSCs as well.[3, 18-22]

Herein, we are reporting for the first time three novel quinacridone (QA) dye based HTMs where we used a common QA central core as acceptor and three different end capping groups donors such as acenaphthylene (ACE), triphenylamine (TPA) and diphenylamine (DPA). All three materials are coded as 2,9-bis(1,2-dihydroacenaphthylen-5-yl)-5,12-dioctyl-5,12-dihydroquinolino[2,3-*b*]acridine-7,14-dione (**ACE-QA-ACE)**, 2,9-bis(4-(bis(4-methoxyphenyl)amino)phenyl)-5,12-dioctyl-5,12-dihydroquinolino[2,3-*b*]acridine-7,14-dione (**TPA-QA-TPA**) and 2,9-bis(bis(4-methoxyphenyl)amino)-5,12-dioctyl-5,12-dihydroquinolino[2,3-*b*]acridine-7,14-dione **(DPA-QA-DPA)**. These HTMs are fully characterized and used as the active hole transporting layers in mesoscopic $TiO_2/CH_3NH_3PbI_3$/HTM solid-state PSCs without using any additives. The aim of this work is to investigate the effect of different end-capping units of QA based HTMs on the PSCs performance. Moreover, the comparison between the efficiency and stability of these new QA based HTMs with the standard 2,2',7,7'-tetrakis(*N*,*N*'-di-pmethoxyphenylamino)-9,9'-spirbiuorene (Spiro-OMeTAD) based devices was also studied.

Results and Discussion

Rational Design and Synthesis

Symmetrical organic semiconductors using planar fused core have been of great benefit to the device performance in optoelectronic applications. Particularly in perovskite solar cells, this kind of geometry is usually used to design organic HTMs because it can improve π–π stacking interactions and high hole mobility.[23-25] In this work, QA polyaromatic hydrocarbon selected as the fused central core because of its planar conjugated structure (resemblance to pentacene with exception of nitrogen and ketonic groups present in the backbone). Additionally strong H-bonding properties provide high charge transport abilities and electron deficient core (acceptor) conjugated backbone plays a role of an allowing a Donor-Acceptor-Donor (D-A-D) geometry, which has recently been shown to provide high performance and stability in PSCs.[26-28] In our current molecular engineering design, we

used QA acceptor as core and ACE, TPA and DPA donor groups as end cappers. TPA and DPA moieties have already been widely used as end-capping groups in the design of organic HTMs for PSCs, and devices using such HTMs displayed not only very high efficiency but also superior stability.[3, 29-33] In contrast, the ACE substituted conjugated HTMs are very rare and our group was the first to report ACE end capping moiety for PSC devices. In our first report, we reported ACE end capped anthranthrone dye which yielded PCE of 13.5% without any additives .[4] Thus, making a series of different end capping units based on QA dye, which are implemented as HTMs in PSCs, will provide a comparative view about the effect of these promising small molecules on the performance and stability of PSCs.

The synthesis routes of **ACE-QA-ACE**, **TPA-QA-TPA** and **DPA-QA-DPA** are illustrated in Scheme 1. The preparation of three precursors, including ACE, TPA and DPA, followed earlier attempts.[3, 4, 19, 29] The target **ACE-QA-ACE** and **TPA-QA-TPA** compounds were synthesized by Suzuki coupling reaction between ACE and TPA boronic ester starting material in combination with common octyl substituted dibromo QA core using a palladium [$Pd(PPh_3)_4$] catalyst and 2M K_2CO_3 base at 120 ^oC for 48 h in the toluene solvent. The synthesis of the target **DPA-QA-DPA** was carried out via Buchwald-Hartwig coupling reaction between dibromo octyl substituted QA and bis(4-methoxyphenyl)amine using tris(dibenzylideneacetone)dipalladium [$Pd_2(dba)_3$] catalyst, tri-tert-butylphosphine ($^tBu_3P$), and sodium tert-butoxide (NaO^tBu) at 110 ^oC for 48 h in anhydrous toluene solvent. After purification, the reaction yield of **ACE-QA-ACE**, **TPA-QA-TPA** and **DPA-QA-DPA** was 62%, 54% and 39%, respectively. The purity of these compounds was verified by proton and C^{13} Nuclear Magnetic Resonance (NMR) spectroscopy (Fig. S1 – S3, Supporting Information (ESI†)). Moreover, the molecular weight of these synthesized materials was confirmed by mass spectroscopy. All these substances are well soluble in most common organic solvents such as chloroform, dichloromethane, and chlorobenzene.

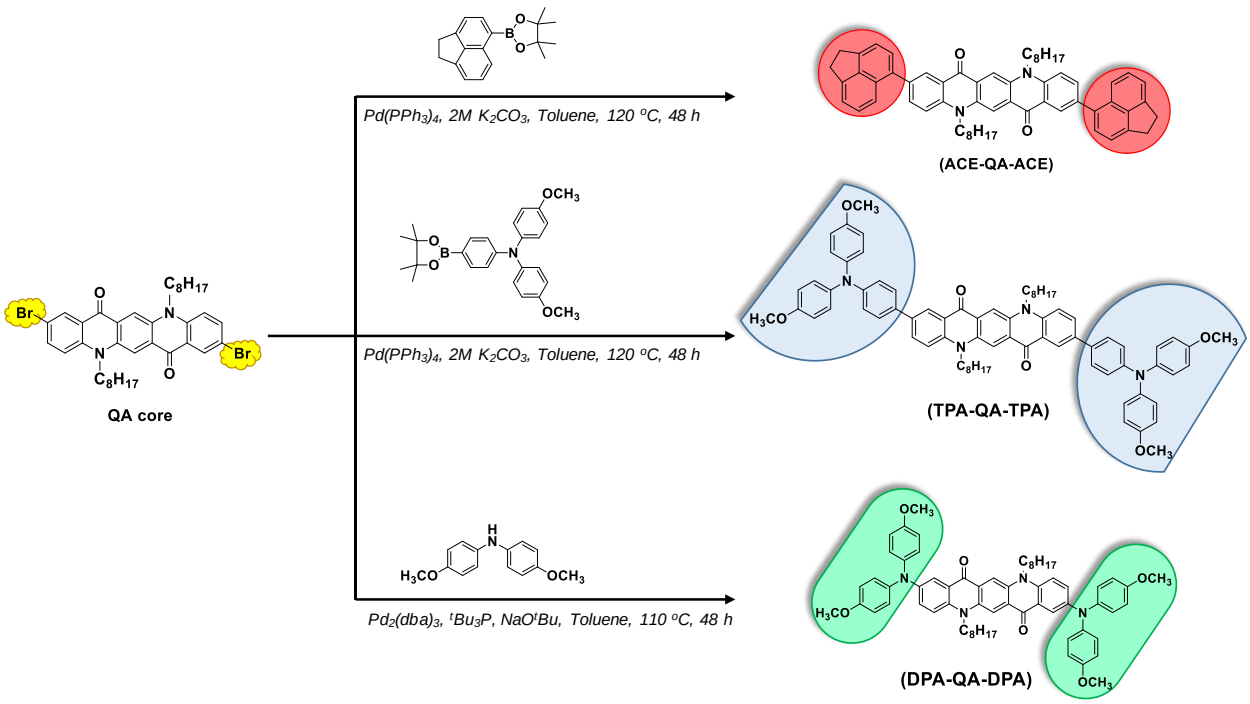

Scheme 1. The synthetic route for QA derivatives. Reagent and conditions: For the synthesis of **ACE-QA-ACE** and **TPA-QA-TPA**: 2M K_2CO_3, toluene, $Pd(PPh_3)_4$, 120 °C, 48 h; For the synthesis of **DPA-QA-DPA**: Diphenylamine, tBu^{3}P, NaOtBu, $Pd_2(dba)_3$, Toluene, 110 °C, 48 h.

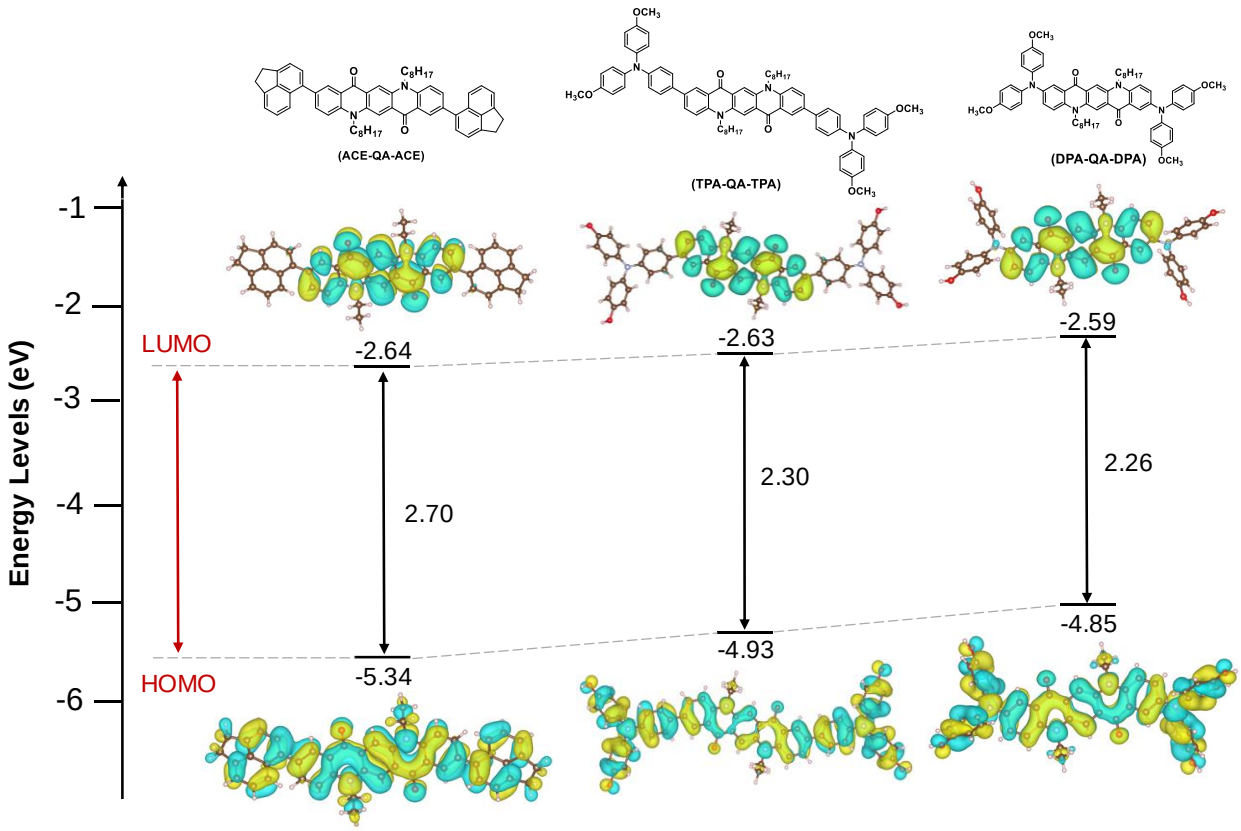

Fig. 1 Calculated electron density of HOMO and LUMO of QA derivatives.

Ab initio Calculations

In order to gain insight about the electron density distribution of key molecular orbitals and their respective energy level trend among molecules, Density Functional Theory (DFT) calculations at the B3LYP level using the basis set Lanl2dz[34-36] and a polarized continuum model of the chloroform solvent[37] were performed. The resulting HOMO and LUMO distributions are displayed in Fig. 1. The trend in HOMO and LUMO energies among the three molecules are similar to that observed experimentally (see below). The computed levels are higher than those measured by PESA likely due to limitations of the approximations used. Generally, three new substances unveil similarities in both electron densities of the HOMO and the LUMO. While the electron distribution of the LUMO is primarily localized on the parent quinacridone skeleton, those of the HOMO are fully delocalized over the entire molecules. This is in good agreement with previous reports.[14, 15, 38] The calculated HOMO values of **ACE-QA-ACE**, **TPA-QA-TPA,** and **DPA-QA-DPA** are -5.34, -4.93 and -4.85 eV, respectively. The LUMO values are -2.64 eV for

ACE-QA-ACE, -2.63 eV for **TPA-QA-TPA,** and -2.59 eV for **DPA-QA-DPA**. Accordingly, the band gap is estimated to be of 2.70 eV for **ACE-QA-ACE**, 2.30 eV for **TPA-QA-TPA,** and 2.26 eV for **DPA-QA-DPA**. In addition to above data, the dihedral angle between end capping ACE and TPA groups with the QA skeleton is computed to be 47° and 28°, respectively whereas the dihedral angle between QA core and end capping DPA group is not observed.

Table 1. Thermal, optical and electrochemical properties of QA derivatives.

HTM	λ_{max} (nm)		λ_{PL} (nm)	Stoke shift (nm)	λ_{onset} (nm)	E_g^{opt} c) (eV)	E_{HOMO} d) (eV)	E_{LUMO} d) (eV)	E_{HOMO} e) (eV)	T_d (°C)	T_g (°C)	T_m (°C)	T_c (°C)	μ ($cm^2V^{-1}s^{-1}$)
	Solution a)	Film b)												
ACE-QA-ACE	301	353	558	257	585	2.12	-5.59	-3.47	-5.37	414	-	265	212	$2.3x10^{-4}$
TPA-QA-TPA	364	368	540	172	626	1.98	-5.41	-3.43	-5.02	424	105	-	-	$1.6x10^{-4}$
DPA-QA-DPA	360	364	-	-	663	1.87	-5.28	-3.41	-4.93	413	74	215	141	$1.2x10^{-4}$

a) Absorption spectrum was measured in chloroform (CF) solution; b) Film was prepared by spin-coating an CF solution containing the sample onto glass substrate at a spin speed of 1000 rpm at room temperature; c) Optical bandgap was calculated from the formula of $1240/\lambda_{onset}$; d) The oxidation potential was measured by photoelectron spectroscopy in air (PESA); $E_{LUMO}^{PESA}=E_{HOMO}^{PESA}+E_g^{opt}$; e) The Oxidation potential of the material was characterized in dichloromethane with 0.1 M tetrabutylammonium hexafluorophosphate at scan speed 100 mV s^{-1}, potentials versus Fc/Fc^+.

Optical Properties

The absorption properties of **ACE-QA-ACE**, **TPA-QA-TPA** and **DPA-QA-DPA** are characterized by UV-Vis spectroscopy. The normalized UV-vis absorption spectra in chloroform (CF) solutions and solid films are shown in Fig. 2a and the data are summarized in Table 1. Generally, a similar pattern of the spectra between CF solutions and thin films is observed, suggesting that there is no significant crystallization in thin films.[29, 39] In addition, the absorption spectra of samples in CF solutions shows the slight blue shift compared to that of thin films, which is mainly caused by the intermolecular interactions in the solid state and the increased π-electron

density (π–π* transitions) of the compound. Obviously, the absorption of **TPA-QA-TPA** is red-shifted compared to that of **DPA-QA-DPA** and **ACE-QA-ACE**, which could be ascribed to the stronger electron-donating ability of TPA unit in comparison with DPA and ACE.[4, 29]

These newly developed materials exhibit three main absorption bands, including 300 – 320 nm, 330 – 400 nm, and 400 – 670 nm. This is in good agreement with previous studies related to other derivatives of QA dyes.[12, 13, 15] The absorption peaks at the region of 300 – 320 nm indicate the absorption of three different end-capping units.[4, 29] Meanwhile, the impact of the intramolecular charge transfer (ICT) between the QA skeleton and end-capping groups results in the prominent peaks at 330 – 400 nm area. Furthermore, their weak additional absorption band at 400 – 670 nm might be caused by ICT between the electron-accepting carbonyl group (C=O) of the parent QA molecule and end-capping groups.[15] In CF solutions, **ACE-QA-ACE** unveils absorption maxima at 301 nm whereas **TPA-QA-TPA** and **DPA-QA-DPA** exhibits at 364 nm and 360 nm respectively. In solid thin film, the absorption peaks of these materials are found to be at 353 nm for **ACE-QA-ACE**, 368 nm for **TPA-QA-TPA** and 364 nm for **DPA-QA-DPA**. Certainly, the optical band gaps calculated by using the absorption onset wavelength (E_g^{opt}=1240/ λ_{onset}) of the corresponding absorption spectrum in solid-state are found 2.12 eV for **ACE-QA-ACE**, 1.98 eV for **TPA-QA-TPA** and 1.87 eV for **DPA-QA-DPA**.

Furthermore, the photoluminescence (PL) spectra in CF and Toluene solutions of these three new materials was carried out and illustrated in Fig. S5 (ESI†) and the results are listed in Table 1. While **DPA-QA-DPA** does not exhibit the emission in CF solution, it shows the emission in Toluene solution which is in good agreement with compound NPh_2-QA in the previous report.[13] On the contrary, the emission maximum of **ACE-QA-ACE** and **TPA-QA-TPA** are found to be 558 nm and 540 nm, respectively. According to the maximum of absorption and emission peaks, the Stoke shift is estimated to be 257 nm for **ACE-QA-ACE**, 172 nm for **TPA-QA-TPA** and 269 nm for **DPA-QA-DPA** taking first strong absorption peak into an account.

Thermal Properties

The thermogravimetric analysis (TGA) and differential scanning calorimetry (DSC) techniques were used to investigate the 5% weight loss and thermal transition of these new materials. This

information will be helpful to determine thermal stability and glass transition temperature, melting temperature and other relevant studies. The corresponding DSC and TGA data are shown in Table 1. According to the TGA curves (Fig. S6, ESI†), the decomposition temperature (T_d) of all these compounds is greater than 410 ^oC, presenting their high thermal stability. The T_d is in the order: **DPA-QA-DPA** (413 ^oC) = **ACE-QA-ACE** (414 ^oC) < **TPA-QA-TPA** (424 ^oC), which is higher than that of original QA skeleton (~370 ^oC).[13, 40] The decomposition temperature of TPA-based HTMs is higher than those of DPA and ACE-based ones, which coincides well with previous studies.[4, 41-43] Thus, the QA cores substituted with ACE, TPA and DPA moieties result in improved thermal stability.

The DSC data (Fig. S7, ESI†) exhibits different glass transition temperatures (T_g), melting temperatures (T_m) and crystalline temperatures (T_c) among these compounds. The T_g of **TPA-QA-TPA** and **DPA-QA-DPA** is found to be 105 ^oC and 74 ^oC, respectively, whereas the T_g of **ACE-QA-ACE** is not observed. For T_m, the values of **ACE-QA-ACE** and **DPA-QA-DPA** are estimated to be 265 ^oC and 215 ^oC, respectively, which is higher than that of original QA skeleton (179 ^oC).[13] Meanwhile, the **TPA-QA-TPA** compound doesn't exhibit T_m and it could be higher than instrument measurement range. Moreover, the T_c of **ACE-QA-ACE** and **DPA-QA-DPA** are assessed to be 212 ^oC and 141 ^oC, respectively, whereas T_c of **TPA-QA-TPA** is not observed. The melting and crystalline behaviors of **TPA-QA-TPA** are not revealed, suggesting that TPA-QA-TPA is a typical amorphous glass. Interestingly, the appearance of methoxy groups in DPA units of **DPA-QA-DPA** leads to the presence of T_c, the decrease in T_d and the increase in both T_m and T_g in comparison with compound NPh_2-QA, which does not possess methoxy ones, in the previous report.[13]

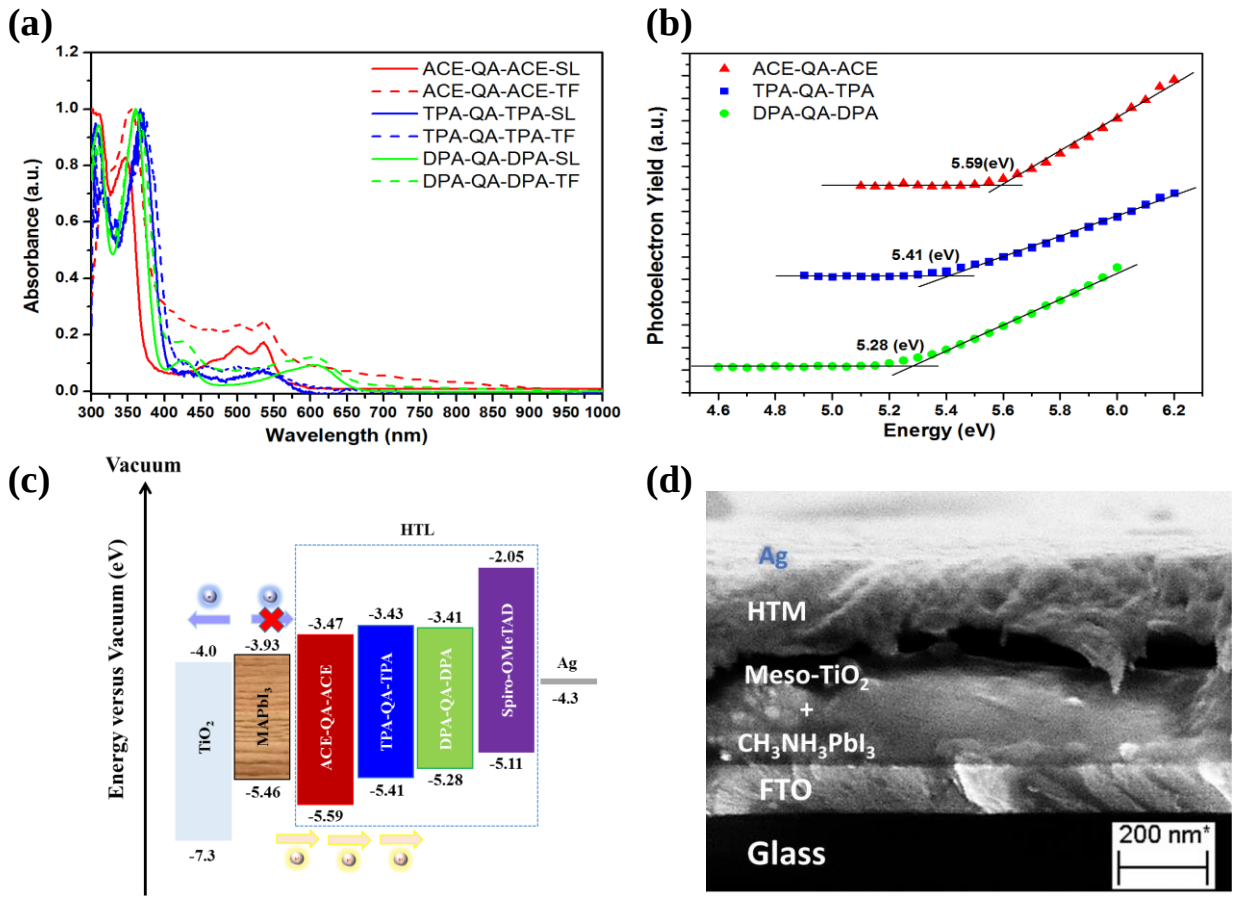

Fig. 2 (a) The UV-Vis absorption and PL spectra in CF solutions and the UV-Vis absorption in films; (b) Photoelectron spectroscopy in air (PESA) spectra; (c) Energy level diagram, (d) Cross-sectional scanning electron microscopy image of PSC of three new materials.

Energy Level Determination

Determining the energy levels of hole transporting materials is quite crucial to estimate the architecture of the device. In this work, the HOMO values of three new materials are measured by photoelectron spectroscopy in air (PESA) (Fig. 2b) and cyclic voltammetry (CV) (Fig. S8, ESI†) methods respectively. The LUMO values of **ACE-QA-ACE**, **TPA-QA-TPA** and **DPA-QA-DPA** are calculated by using the difference between the HOMO values and the optical band gap via the equation: $E_{\mathrm{LUMO}}^{\mathrm{PESA}}=E_{\mathrm{HOMO}}^{\mathrm{PESA}}+E_g^{opt}$. The corresponding data are shown in Table 1. In this report, the energy values based on PESA data was used instead of CV one because the PESA measurements were done in the thin film forms, which are more relevant to the actual devices.[3, 4] As shown in

Fig. 2b, the HOMO values of **ACE-QA-ACE**, **TPA-QA-TPA** and **DPA-QA-DPA** are assessed to be at -5.59 eV, -5.41 eV and -5.28 eV, respectively. These HOMO values are deeper than that of Spiro-OMeTAD (-5.22 eV)[19, 44] which may lead to more efficient hole-transport ability than conventional Spiro-OMeTAD. The substitution of three different terminating units ACE, TPA and DPA has impacted the low-lying HOMO energy level, proving that the strong electron donating ability displays an order of ACE > TPA > DPA. The stronger electron donating ability of TPA compared to DPA coincides well with the experimental red shifts in UV-Vis spectra of both compounds and the trend observed for the energy levels of other HTMs based on these end-capping moieties in the earlier attempts.[29, 42, 43, 45, 46] On the contrary, in case of ACE unit, it is not in good accordance with the previous report.[4] This may be attributed to the weak electron donating ability of QA core in comparison with the strong electron donating ability of ANT one arising from more extended conjugated nature of the core. According to the HOMO values and the optical band gap, the obtained LUMO value is found to be -3.47 eV for **ACE-QA-ACE**, -3.43 eV for **TPA-QA-TPA** and -3.41 eV for **DPA-QA-DPA**. These LUMO offset between active perovskite layer and hole transporting material is quite low and this will block the electron movement, which can cause boosting the solar cell efficiency.

Perovskite Solar Cells

The new QA core based small molecules were employed as hole transport materials in the typical mesoporous perovskite solar cells with $TiO_2/CH_3NH_3PbI_3$/HTM/Ag device architecture. This device architecture allows us to investigate the effect of different end-capping groups on the performance of perovskite solar cells.

The mesoporous devices were prepared using the previously reported procedure [47, 48] which is described in the experimental section above. A compact TiO_2 layer of around 30-40 nm thickness is first deposited on the conducting FTO substrate by spray pyrolysis, then a mesoporous TiO_2 is deposited by using the conventional spin-coating methodology. The $CH_3NH_3PbI_3$ absorber is then spin-coated using anti solvent treatment. The perovskite solution was prepared by dissolving 50 wt % of $CH_3NH_3PbI_3$ in the mixed dimethyl sulfoxide and gamma butyrolactone (GBL). The sample was annealed for 30 minutes at 100 ^oC. Once the substrate cooled down, a hole transport

layer of 100-120 nm was applied on top of the $CH_3NH_3PbI_3$. At last, the silver (Ag) as a counter electrode was deposited by thermal evaporation.

The $TiO_2/CH_3NH_3PbI_3$/HTM/Ag architecture of the PSC devices were kept constant and just the hole transport layers are changed. This allows to isolate the effect of the different HTMs used. The optimized, champion device efficiency and the corresponding photovoltaic performance for all three different dopant-free HTMs and conventional doped Spiro-OMeTAD are shown in Fig. 3 and Table 2, respectively. According to Fig. 3a, the non-doped **ACE-QA-ACE** HTM based PSC devices show a record PCE of 18.2% (J_{sc}=22.41 mA cm^{-2}, V_{oc}=1.06 V and FF=77%) whereas lower PCEs are obtained from the devices using **TPA-QA-TPA** and **DPA-QA-DPA** HTMs under similar conditions. The **TPA-QA-TPA** HTM based PSCs yields a PCE of 16.6% (J_{sc}=22.4 mA cm^{-2}, V_{oc}=0.99 V and FF=75.1%) whereas those of **DPA-QA-DPA** HTM displays a PCE of 15.5% (J_{sc}=22.38 mA cm^{-2}, V_{oc}=0.95 V and FF=73.2%). Meanwhile, the control devices based on doped Spiro-OMeTAD show an efficiency of 15.2% with a J_{sc} of 21.46 mA cm^{-2}, a V_{oc} of 1.03 V and a FF of 69.3%. Additionally, all devices made employing different HTMs exhibited very little hysteresis (Fig. S9, ESI†). The excessive small band offset between perovskite and the HTL hampers the effective hole transport ability. Our result shows that the higher V_{oc} (1.06 V) obtained by employing **ACE-QA-ACE** HTMs as compared to lower V_{oc} of 0.99 V and 0.95 V obtained by using **TPA-QA-TPA** and **DPA-QA-DPA** respectively, is a result of small band offset and HOMO value difference between these HTMs and perovskite absorber.[49-51] Moreover, the dopant free **ACE-QA-ACE** HTM based PSCs shows negligible change in short circuit current (J_{sc} = 22.41 mA cm^{-2}) compared to the **TPA-QA-TPA** (J_{sc} = 22.40 mA cm^{-2}) and **DPA-QA-DPA** (J_{sc} = 22.38 mA cm^{-2}). This is due to the shallow HOMO of all QA core based HTMs that allows effective hole transport.

The device performance of these new HTMs based devices is in order: **DPA-QA-DPA** < **TPA-QA-TPA** < **ACE-QA-ACE**. The efficiency of **TPA-QA-TPA** HTL based devices is higher than that of **DPA-QA-DPA**, which is in agreement with previous attempts reporting that the PCE obtained using TPA terminating groups-based HTMs is greater than that with DPA in mesoporous layouts under similar characterization conditions.[29, 41, 42, 46, 52, 53] Furthermore, the PCE of **ACE-QA-ACE** HTM-based devices is better than those of **TPA-QA-TPA**, which does not agree well with an earlier study.[4] This could be ascribed to the different electron accepting/donating ability of quinacridone and anthanthrone cores. Though both the quinacridone and anthanthrone contains

two ketonics (C=O) groups but anthanthrone is more fused aromatic with extended conjugation, which possesses more electron donating capability than quinacridone.

The space charge limited current (SCLC) method was used to measure the hole transport properties of different hole transport layers. For these measurements, HTMs were spin-coated on top of ITO/PEDOT:PSS substrate and then gold metal contacts were deposited on top by thermal evaporation process. The work function of ITO and gold are close enough to that of the HTMs HOMO level hence this whole assembly acts as a hole-only device from which the mobility can be determined (Table 1 and Fig. S10, ESI†). The highest hole mobility of 2.3 x 10^{-4} cm^2 $V^{-1}s^{-1}$ was obtained for **ACE-QA-ACE** and was higher than that of **TPA-QA-TPA** (1.6 x 10^{-4} cm^2 $V^{-1}s^{-1}$), **DPA-QA-DPA** (1.2 x 10^{-4} cm^2 $V^{-1}s^{-1}$) and doped Spiro-OMeTAD (1.4 x 10^{-4} cm^2 $V^{-1}s^{-1}$). This trend of effective hole transport is well matched with the efficiency obtained employing these HTMs.

As shown in Fig. 3b, the devices with **ACE-QA-ACE** HTL exhibit an incident photon-to-current efficiency (IPCE) values around 80-90% from 360 to 650 nm covering the entire UV region with the highest IPCE of 90% observed at 540 nm. The integrated current density calculated from IPCE spectrum presented in Figure 3(b) is in well match to the current density (*Jsc)* values obtained from the IV curves (Figure 3(a))

The maximum power point tracking with each HTM is displayed in Fig. 3c. In comparison with other organic dyes employed as small molecular HTMs for perovskite solar cells (Table S2, ESI†), the power conversion efficiency of 18.2% obtained using dopant-free **ACE-QA-ACE** HTM here is the highest reported efficiency. The PSCs prepared using **ACE-QA-ACE**, **TPA-QA-TPA**, **DPA-QA-DPA** and Spiro-OMeTAD show an average device efficiency of 14.7%, 13.0%, 12.1% and 11.4% respectively as shown in Table 2.

Perovskite solar cells suffer from rapid degradation when exposed to high humidity conditions. Therefore, a PSCs stability measurement in high humidity is an important aspect to evaluate further. We have kept all our champion devices for 720 hours in 75% relative humidity and checked their performance at regular intervals. Fig. 3d shows aging of perovskite solar cells. PSC made with dopant-free HTMs (**ACE-QA-ACE**, **TPA-QA-TPA** and **DPA-QA-DPA**) shows improved stability over devices prepared using doped Spiro-OMeTAD. In our previous study, the fast degradation of the solar cells which were doped with LiTFSI salt was explained.[4]

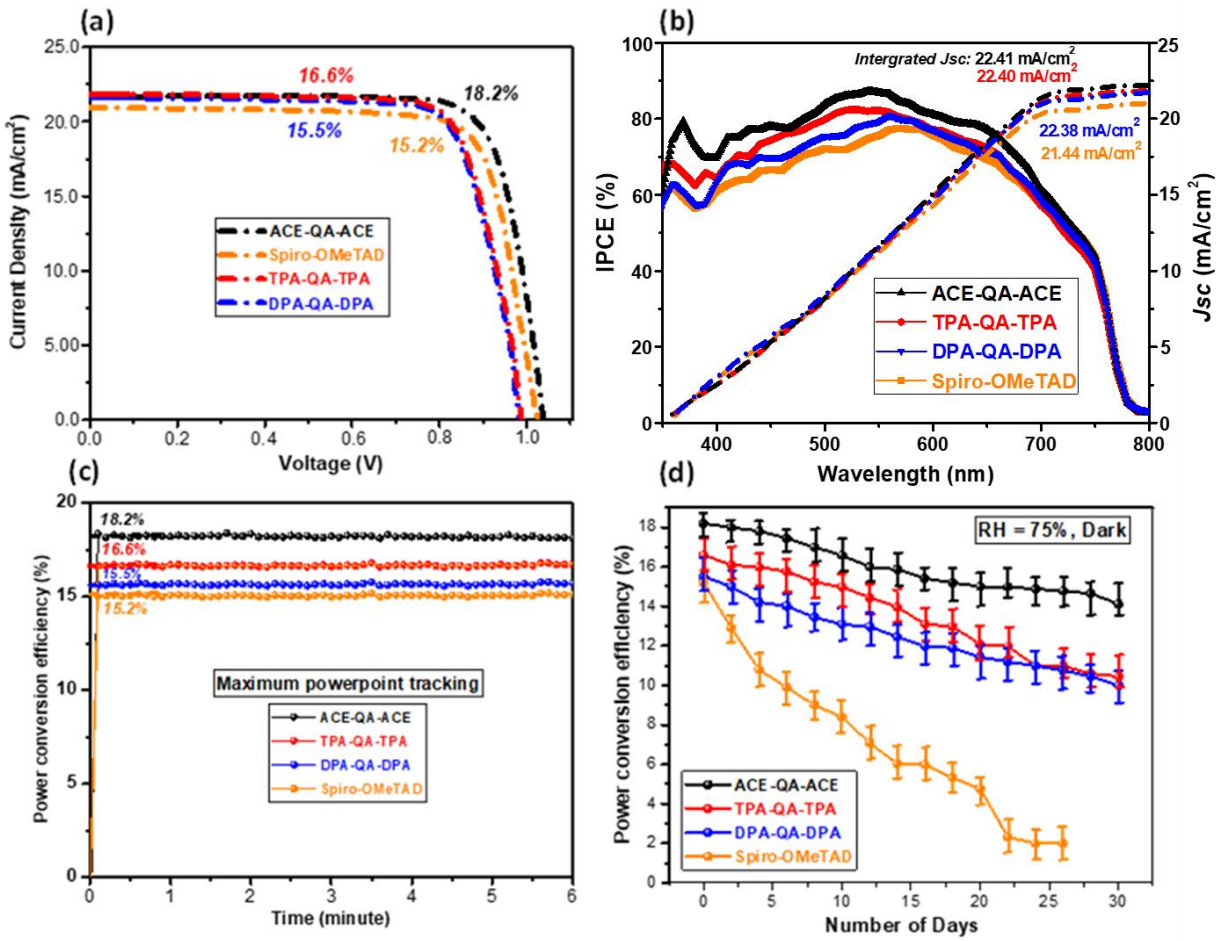

Fig. 3 (a) Photovoltaic performance of perovskite devices prepared using Spiro-OMeTAD and QA derivatives HTMs, respectively illumination; (b) Absolute IPCE spectra (solid line) and integrated current density calculated for optimized PSCs prepared using different hole transporting layers; (c) Power output under maximum power point tracking for 360 s, starting from forward bias and resulting in a stabilized power output of 18.2, 16.6, 15.5 and 15.2% for **ACE-QA-ACE**, **TPA-QA-TPA**, **DPA-QA-DPA** and Spiro-OMeTAD - based devices, respectively. The devices measured at voltage scan rate of 10 mV s^{-1}; (d) Aging of champion devices stored in high relative humidity of 75% and in dark condition for 725 hours (30 days).

Table 2 Solar cell device performance with different HTMs under 1 sun condition.

HTLs[a)]	Scan Direction	V_{OC} [V]	J_{SC} [mA/cm^2]	FF [%]	PCE [%]
ACE-QA-ACE	Forward	1.06	22.41	77.0	18.2
	Reverse	1.06	22.36	76.7	18.0
	Average[c)]	1.00	20.32	72.5	14.7
TPA-QA-TPA	Forward	0.99	22.40	75.1	16.6
	Reverse	0.98	22.34	75.0	16.0
	Average[c)]	0.95	20.00	69.6	13.0
DPA-QA-DPA	Forward	0.95	22.38	73.2	15.5
	Reverse	0.95	22.34	73.0	15.2
	Average[c)]	0.91	19.70	68.1	12.1
Doped Spiro-OMeTAD[b)]	Forward	1.03	21.46	69.3	15.2
	Reverse	1.02	21.35	68.4	14.8
	Average[c)]	0.93	19.00	65.0	11.4

[a)] Cell size (active area): 0.100 cm^2. Photovoltaic performance at 1000 Wm^{-2} (AM1.5G) and constant scan speed of 10 mVs^{-1} mesoscopic $MAPbI_3$ devices; [b)]with additives: 4-tert-butylpyridine (*t*BP) and Li-bis(trifluoromethanesulfonyl)-imide (LiTFSI); [c)]An average device efficiency of a total of 40 devices for each Spiro-OMeTAD and QA derivatives, respectively (Fig. S11, ESI†).

Conclusions

In summary, three novel small molecular hole transporting materials based on quinacridone dye, namely **ACE-QA-ACE**, **TPA-QA-TPA** and **DPA-QA-DPA**, were designed, synthesized and characterized successfully. For the first time, they were employed as dopant-free HTMs in the mesoporous perovskite solar cells. In comparison with that of the standard doped Spiro-OMeTAD (15.2%), the perovskite cells prepared using pristine newly developed **ACE-QA-ACE**, **TPA-QA-TPA,** and **DPA-QA-DPA** HTMs yielded 18.2%, 16.6% and 15.5%, respectively under 1 sun condition. The resultant devices of new HTMs exhibited negligible hysteresis. As a result of avoiding the use of hygroscopic LiTFSI and TBP additives in our novel hole transport material, the stability of non-encapsulated devices improved significantly vs that of doped Spiro-OMeTAD under similar aging conditions. The champion devices using **ACE-QA-ACE** HTL achieved the highest PCE and retained superior stability to other HTMs due to its higher hole mobility and suitable energy levels. The outstanding result proves that the newly developed HTMs based on quinacridone dyes can boost the efficiency and stability of perovskite solar cell devices.

Experimental

Detailed experimental methods can be found in the Supporting Information.

Conflicts of interest

There are no conflicts to declare.

Acknowledgements

H.D.P and S.M.J. share equal contribution for this work. H.D.P is thankful to QUT for offering here QUTPRA scholarship to conduct his research work. Some of the data reported in this paper were obtained at the Central Analytical Research Facility operated by the Institute for Future Environments (QUT). Access to CARF is supported by generous funding from the Science and Engineering Faculty (QUT). Author S. M. J. is thankful to Welsh assembly Government funded Sêr Cymru Solar project, EPSRC grants EPSRC Supergen SuperSolar Hub for an International and Industrial Engagement Award (Supergen Solar Challenge) and Marie-Curie COFUND fellowship for financial support. The UKRI Global Challenge Research Fund project SUNRISE (EP/P032591/1). S.M. is supported by the Ministry of Education of Singapore. Additionally, this project has received funding from the European Union's Horizon 2020 research and innovation programme under the Marie Skłodowska-Curie grant agreement No 663830. N.M. acknowledges the support of the Queensland government via the Q-CAS funding scheme. P.S. is thankful to QUT for financial support and to the Australian Research Council for the Future Fellowship grant FT130101337.

References

1. J.-F. Morin, *J. Mater. Chem. C*, 2017, **5**, 12298-12307.
2. C. Wang, Z. Zhang and Y. Wang, *J. Mater. Chem. C*, 2016, **4**, 9918-9936.
3. H. D. Pham, K. Hayasake, J. Kim, T. T. Do, H. Matsui, S. Manzhos, K. Feron, S. Tokito, T. Watson, W. C. Tsoi, N. Motta, J. R. Durrant, S. M. Jain and P. Sonar, *J. Mater. Chem. C*, 2018, **6**, 3699-3708.
4. H. D. Pham, T. T. Do, J. Kim, C. Charbonneau, S. Manzhos, K. Feron, W. C. Tsoi, J. R. Durrant, S. M. Jain and P. Sonar, *Adv. Energy Mater.*, 2018, **8**, 1703007.
5. T. T. Do, K. Rundel, Q. Gu, E. Gann, S. Manzhos, K. Feron, J. Bell, C. R. McNeill and P. Sonar, *New J. Chem.*, 2017, **41**, 2899-2909.
6. C. Yin, J. Lu, Y. Xu, Y. Yun, K. Wang, J. Li, L. Jiang, J. Sun, A. D. Scully, F. Huang, J. Zhong, J. Wang, Y.-B. Cheng, T. Qin and W. Huang, *Adv. Energy Mater.*, 2018, DOI: 10.1002/aenm.201800538.
7. T.-T. Bui, M. Ulfa, F. Maschietto, A. Ottochian, M.-P. Nghiêm, I. Ciofini, F. Goubard and T. Pauporté, *Org. Electron.*, 2018, **60**, 22-30.
8. X. Yina, L. Guan, J. Yua, D. Zhao, C. Wang, Niraj Shresthab, Y. Han, Q. An, J. Zhou, B. Zhou, Y. Yu, C. R. Grice, R. A. Awni, F. Zhang, J. Wang, R. J. Ellingson, Y. Yan and W. Tang, *Nano Energy*, 2017, **40**, 163-169.
9. S.-H. Peng, T.-W. Huang, G. Gollavelli and C.-S. Hsu, *J. Mater. Chem. C*, 2017, **5**, 5193-5198.
10. Y. S. Kwon, J. Lim, H.-J. Yun, Y.-H. Kim and T. Park, *Energy Environ. Sci.*, 2014, **7**, 1454-1460.
11. C.-H. Tsai, N. Li, C.-C. Lee, H.-C. Wu, Z. Zhu, L. Wang, W.-C. Chen, H. Yan and C.-C. Chueh, *J. Mater. Chem. A*, 2018, **6**, 12999-13004.
12. T. Zhou, T. Jia, B. Kang, F. Li, M. Fahlman and Y. Wang, *Adv. Energy Mater.*, 2011, **1**, 431–439.
13. C. Wang, S. Wang, W. Chen, Z. Zhang, H. Zhang and Y. Wang, *RSC Adv.*, 2016, **6**, 19308-19313.
14. M. P. d. Cunha, T. T. Do, S. D. Yambem, H. D. Pham, S. Chang, S. Manzhos, R. Katoh and P. Sonar, *Mater. Chem. Phys.*, 2018, **206**, 56-63.
15. J. Jia, C. Hu, Y. Cui, Y. Li, W. Wang, L. Han, Y. Li and J. Gao, *Dyes Pigm.*, 2018, **149**, 843-850.
16. Y. Qu, Y. Jin, Y. Cheng, L. Wang, J. Cao and J. Yang, *J. Mater. Chem. A*, 2017, **5**, 14537-14541.
17. T. L. Chen, J. J.-A. Chen, L. Catane and B. Ma, *Org. Electron.*, 2011, **12**, 1126-1131.
18. K. Liu, Y. Yao, J. Wang, L. Zhu, M. Sun, B. Ren, L. Xie, Y. Luo, Q. Meng and X. Zhan, *Mater. Chem. Front.*, 2017, **1**, 100-110.

19. H. D. Pham, Z. Wu, L. K. Ono, S. Manzhos, K. Feron, N. Motta, Y. Qi and P. Sonar, *Adv. Electronic Mater.*, 2017, **3**, 1700139.

20. P. Ganesan, K. Fu, P. Gao, I. Raabe, K. Schenk, R. Scopelliti, J. Luo, L. H. Wong, M. Grätzel and M. K. Nazeeruddin, *Energy Environ. Sci.*, 2015, **8**, 1986-1991.

21. S. Park, J. H. Heo, C. H. Cheon, H. Kim, S. H. Im and H. J. Son, *J. Mater. Chem. A*, 2015, **3**, 24215-24220.

22. K. Do, H. Choi, K. Lim, H. Jo, J. W. Cho, M. K. Nazeeruddin and J. Ko, *Chem. Commun.*, 2014, **50**, 10971-10974.

23. M. Cheng, B. Xu, C. Chen, X. Yang, F. Zhang, Q. Tan, Y. Hua, L. Kloo and L. Sun, *Adv. Energy Mater.*, 2015, **5**, 1401720-1401728.

24. Q. Liu, A. Surendran, K. Feron, S. Manzhos, X. Jiao, C. R. McNeill, S. E. Bottle, J. Bell, W. L. Leong and P. Sonar, *New J. Chem.*, 2018, **42**, 4017-4028.

25. W. Wu, Y. Liu and D. Zhu, *Chem. Soc. Rev.*, 2010, **39**, 1489-1502.

26. H. Zhang, Y. Wu, W. Zhang, E. Li, C. Shen, H. Jiang, H. Tian and W.-H. Zhu, *Chem. Sci.*, 2018, DOI: 10.1039/c8sc00731d.

27. P. Xu, P. Liu, Y. Li, B. Xu, L. Kloo, L. Sun and Y. Hua, *ACS Appl. Mater. Interfaces*, 2018, **10**, 19697-19703.

28. Y. C. Chen, S. K. Huang, S. S. Li, Y. Y. Tsai, C. P. Chen, C. W. Chen and Y. J. Chang, *ChemSusChem*, 2018, DOI: 10.1002/cssc.201801258.

29. H. D. Pham, H. Hu, F.-L. Wong, C.-S. Lee, W.-C. Chen, K. Feron, S. Manzhos, H. Wang, N. Motta, Y. M. Lam and P. Sonar, *J. Mater. Chem. C*, 2018, **6**, 9017-9029.

30. H. D. Pham, H. Hu, K. Feron, S. Manzhos, H. Wang, Y. M. Lam and P. Sonar, *Sol. RRL*, 2017, **1**, 1700105.

31. M. Saliba, S. Orlandi, T. Matsui, S. Aghazada, M. Cavazzini, J.-P. Correa-Baena, P. Gao, R. Scopelliti, E. Mosconi, K.-H. Dahmen, F. De Angelis, A. Abate, A. Hagfeldt, G. Pozzi, M. Graetzel and M. K. Nazeeruddin, *Nat. Energy*, 2016, **1**, 15017-15024.

32. T. H. Le, Q. D. Dao, M. P. Nghiem, S. Peralta, R. Guillot, Q. N. Pham, A. Fujii, M. Ozaki, F. Goubard and T. T. Bui, *Chem. Asian J.*, 2018, **13**, 1302-1311.

33. D. E. M. Rojas, K. T. Cho, Y. Zhang, M. Urbani, N. Tabet, G. de la Torre, M. K. Nazeeruddin and T. Torres, *Adv. Energy Mater.*, 2018, DOI: 10.1002/aenm.201800681.

34. A. D. Becke, *J. Chem. Phys.*, 1993, **98**, 5648-5652.

35. P. Hohenberg and W. Kohn, *Phys. Rev.* , 1964, **136**, B864-B871.

36. W. Kohn and L. Sham, *Phys. Rev.* , 1965, **140**, A1133-A1138.

37. J. Tomasi, B. Mennucci and R. Cammi, *Chem. Rev.*, 2005, **105**, 2999-3094.

38. J. Jia, Y. Li, W. Wang, C. Luo, L. Han, Y. Li and J. Gao, *Dyes Pigm.*, 2017, **146**, 251-262.

39. J. Wang, S. Wang, X. Li, L. Zhu, Q. Meng, Y. Xiao and D. Li, *Chem. Commun.*, 2014, **50**, 5829-5832.

40. Z.-X. Xu, H.-F. Xiang, V. A. L. Roy, S. S.-Y. Chui, Y. Wang, P. T. Lai and C.-M. Che, *Appl. Phys. Lett.*, 2009, **95**, 123305.

41. A. Molina-Ontoria, I. Zimmermann, I. Garcia-Benito, P. Gratia, C. Roldan-Carmona, S. Aghazada, M. Graetzel, M. K. Nazeeruddin and N. Martin, *Angew. Chem. Int. Ed. Engl.*, 2016, **55**, 6270-6274.

42. R. Grisorio, B. Roose, S. Colella, A. Listorti, G. P. Suranna and A. Abate, *ACS Energy Lett.*, 2017, **2**, 1029-1034.

43. R. Grisorio, R. Iacobellis, A. Listorti, L. De Marco, M. P. Cipolla, M. Manca, A. Rizzo, A. Abate, G. Gigli and G. P. Suranna, *ACS Appl. Mater. Interfaces*, 2017, **9**, 24778-24787.

44. N. J. Jeon, H. G. Lee, Y. C. Kim, J. Seo, J. H. Noh, J. Lee and S. I. Seok, *J. Am. Chem. Soc.*, 2014, **136**, 7837-7840.

45. R. Azmi, S. Y. Nam, S. Sinaga, Z. A. Akbar, C.-L. Lee, S. C. Yoon, I. H. Jung and S.-Y. Jang, *Nano Energy*, 2018, **44**, 191-198.

46. X. Liu, F. Kong, R. Ghadari, S. Jin, T. Yu, W. Chen, G. Liu, Z. Tan, J. Chen and S. Dai, *Chem. Commun.*, 2017, **53**, 9558-9561.

47. S. M. Jain, Z. Qiu, L. Häggman, M. Mirmohades, M. B. Johansson, T. Edvinsson and G. Boschloo, *Energy Environ. Sci.*, 2016, **9**, 3770-3782.

48. S. M. Jain, B. Philippe, E. M. J. Johansson, B.-w. Park, H. Rensmo, T. Edvinsson and G. Boschloo, *J. Mater. Chem. A*, 2016, **4**, 2630-2642.

49. W.-J. Yin, J.-H. Yang, J. Kang, Y. Yan and S.-H. Wei, *J. Mater. Chem. A*, 2015, **3**, 8926-8942.

50. Z. Liu, K. Liu, H. Wang, S. M. Jain, J. Duan, T. He, R. Fan, J. Yang, H. Liu and F. Zhang, *Solar Energy*, 2018, **176**, 1-9.

51. M. Li, Z. K. Wang, M. P. Zhuo, Y. Hu, K. H. Hu, Q. Q. Ye, S. M. Jain, Y. G. Yang, X. Y. Gao and L. S. Liao, *Adv. Mater.*, 2018, **30**, 1800258.

52. A. Krishna, D. Sabba, H. Li, J. Yin, P. P. Boix, C. Soci, S. G. Mhaisalkar and A. C. Grimsdale, *Chem. Sci.*, 2014, **5**, 2702-2709.

53. X. Liu, F. Kong, T. Cheng, W. Chen, Z. Tan, T. Yu, F. Guo, J. Chen, J. Yao and S. Dai, *ChemSusChem.*, 2017, **10**, 968-975.

Table of Content Figure

A series of novel pristine hole transporting materials-based quinacridone (QA) dyes is developed and fabricated in mesoporous perovskite solar cells in the first time. Among them, the devices using QA core with acenaphthylene (ACE) moieties as terminating units, namely ACE-QA-ACE, exhibits highest performance with 18.2% efficiency. The resultant devices show the outstanding efficiency of these new materials and superior stability compared to those of the standard doped Spiro-OMeTAD ones.